ORIGINAL RESEARCH ARTICLE

Influence of Thickness and Ti Interlayer on Scratch and Wear Resistance of CoCrNi Medium Entropy Alloy Coatings

Fuyang Cao, Haoquan Wang, Jiayi Xie, Zhanliang Hao, Rui Luo, Zhizhong Yuan, Zhifeng Zhou, Zonghan Xie, and Paul Munroe

Submitted: 20 February 2024 / Revised: 7 April 2024 / Accepted: 3 May 2024

CoCrNi-based medium entropy alloys (MEAs), as one of the derivatives of the Cantor (FeNiCoCrMn) high entropy alloy, have attracted extensive research interest due to their remarkable mechanical properties and outstanding radiation and corrosion resistance. In this work, scratch and wear testing was carried out on various MEA CoCrNi coatings (of different thicknesses, both with, or without, the presence of a Ti interlayer) to study the effects of both coating thickness and the inclusion of the Ti interlayer on scratch adhesion strength and wear performance. For the MEA coatings directly deposited onto the substrates, the coating adhesion strength weakened with an increase in coating thickness. Counterintuitively, the introduction of a Ti interlayer was found to be detrimental for the scratch adhesion strength compared with the samples prepared without an interlayer, where severe surface fracture was observed for the thicker MEA CoCrNi coatings. Additionally, the wear results show that thinner CoCrNi or CoCrNi/Ti coatings demonstrate better wear resistance than their thicker counterparts. It is believed that the residual compressive stresses present in these coatings contribute a significant role in influencing their wear performance.

Keywords adhesion strength, CoCrNi, medium entropy alloys, scratch, wear performance

1. Introduction

High entropy alloys (HEAs), which are commonly defined to consist of five or more principal metal elements with each element having a concentration ranging from 5 to 35 at.%, have recently generated extensive attention due to their appealing properties and potential applications (Ref 1-7). Following the initial discovery of HEAs, ternary systems, referred to as medium entropy alloys (MEAs), have emerged. CoCrNi, as one of the most investigated MEAs, exhibits very attractive tensile behavior and fracture toughness under cryogenic conditions, exceeding those of the majority of both HEAs and MEAs. Recent studies have shown that the exceptional mechanical

Fuyang Cao, School of Materials Science and Engineering, Jiangsu University, Zhenjiang 212013, China; and School of Materials Science and Engineering, UNSW Sydney, Sydney, NSW 2052, Australia; Haoquan Wang, Jiayi Xie, Zhanliang Hao, Rui Luo, and Zhizhong Yuan, School of Materials Science and Engineering, Jiangsu University, Zhenjiang 212013, China; Zhifeng Zhou, Hong Kong Branch of National Precious Metals Material Engineering Research Centre (NPMM), City University of Hong Kong, Kowloon, Hong Kong, China; Zonghan Xie, School of Mechanical Engineering, University of Adelaide, Adelaide, SA 5005, Australia; and School of Engineering, Edith Cowan University, Joondalup, WA 6027, Australia; and Paul Munroe, School of Materials Science and Engineering, UNSW Sydney, Sydney, NSW 2052, Australia. Contact e-mail: fuyangcao@ujs.edu.cn.

properties of the single face-centered cubic (FCC) phase CoCrNi MEA can be attributed to the effects of twinning induced plasticity (Ref 8-12), leading to the formation of a 3D twinned structure following deformation. This composition also exhibits excellent resistance to environmental degradation due to the high concentration of corrosion-resistant elements (Cr and Ni) (Ref 2). More recently, modifications such as the addition of gadolinium (Ref 10) or the incorporation of second phases, such as h-BN to form CoCrNi/h-BN composites (Ref 9), have been proposed with the objective to further enhance the mechanical properties of CoCrNi-based alloys.

Most HEAs (as well as MEAs) are fabricated in bulk form through methods such as arc melting, casting, vacuum induction melting and powder metallurgy, which incur high costs of both raw materials and energy (Ref 8). Investigations concerning the deposition of high-performance HEAs and MEAs thin films on to low-cost metal substrates have attracted recent interest (Ref 3-6). In addition to cost efficiency, these films also exhibit excellent mechanical properties, compared to their bulk counterparts. Recently, several techniques have been used to prepare HEA and MEA films and coatings, including magnetron sputtering, laser cladding, thermal spray, etc. (Ref 13-19).

Since adhesion is one of the key issues in the performance of coatings, it is a common strategy to enhance adhesion strength at the coating-substrate interface, particularly for nitride hard coatings, by incorporating a metallic interlayer, such as elemental materials like Ti or Cr (Ref 20, 21). For instance, Bull et al. determined the effect of a Ti interlayer on the adhesion behavior of TiN coatings (Ref 22). They attributed the enhanced adhesion strength of the TiN coatings that incorporated a Ti interlayer, to the effects of chemical getting and mechanical compliance of the soft Ti layer. That is, firstly,

Published online: 17 June 2024

the interlayer can lead to the dissolution of the residual oxide layer present on the surface of the substrate. Secondly, it is evident that the metallic interlayer can act as a relatively soft compliant layer to reduce the shear stress across the coating-substrate interface and so hinder crack propagation in the interfacial region. Additionally, a number of investigations have been performed to study the effect of interlayer thickness on the mechanical behavior, residual stress, adhesion and toughness of nitride-based coating systems (Ref 20).

In addition to the presence of interlayers, coating thickness is also one of the critical parameters which affects the degree of residual stress present in physical vapor deposited (PVD) coatings. This, in turn, influences the stress field distribution under contact loading. It is suggested that there may be an optimal coating thickness to maximize performance since the PVD coating microstructure and mechanical behavior are dependent on thickness (Ref 22, 23).

In our previous investigation, MEA CoCrNi coatings of different thickness were deposited onto AISI M2 steel substrate using a DC magnetron sputtering system. The incorporation of a titanium interlayer in these coatings was shown to induce grain refinement leading to a structure of fine columnar grains (Ref 1, 2). Nanoindentation results showed that the coating thickness had marginal effect on both hardness and elastic modulus of the CoCrNi coatings. However, an incorporation of a Ti interlayer into the CoCrNi coatings led to a marginal decrease in both values. Further, coating thickness was shown to affect the integrity of the coating system under loading, especially for the thicker MEA CoCrNi coatings either with or without the Ti interlayer. Zhao et al. investigated the wear behavior of a CoCrNi medium entropy alloy coating deposited onto 5083Al alloy substrate by resistance seam processing (Ref 24). They showed that the mean hardness of the MEA coating was 775 HV $_{0.2}$ and the average wear rate of the MEA CoCrNi coating was 2.47×10^{-4} mm 3 /Nm, which was ~10 times larger than that of the uncoated alloy. Further, Pan et al. reported the wear response of fine-grained CoCrNi MEA against Inconel counterparts at temperatures between room temperature and 300 °C. They determined that the wear rate decreased as temperature increased and attributed the reduced wear rates and friction coefficient to the formation of surface layer generated through a tribo-chemical process (Ref 11). However, the effects of parameters such as coating thickness or the presence of a Ti interlayer on the scratch adhesion strength and wear performance of MEA CoCrNi coatings have not been investigated. In the present work, we report on the scratch response and wear behavior of MEA CoCrNi coatings, 1 and 3 μ m in thickness, both with and without an incorporation of Ti interlayer. The underlying mechanisms determining the scratch and wear response of the CoCrNi coatings are discussed.

2. Experimental Details

MEA CoCrNi coatings were deposited onto AISI M2 steel substrates via a DC magnetron sputtering system. The CoCrNi target current (DC) was maintained at 4.0 A (sputtering power ~ 1.5 kW), corresponding to a nominal deposition rate of ~ 72 nm/min. Two CoCrNi coatings with nominal thicknesses of 1 and 3 μm were deposited directly onto the steel substrate. These two coatings were referred to as CoCrNi1 and CoCrNi3, respectively. The Ti target current (DC) was set at 4.0 A

(sputtering power ~ 1 kW), corresponding a nominal deposition rate of 10 nm/min. A further two CoCrNi coatings, of the same thickness, that also included a Ti wetting layer with a thickness of ~ 150 nm were also prepared. These two coatings are here after referred to as CoCrNi1/Ti and CoCrNi3/Ti, respectively. A detailed description of the deposition conditions, microstructural and mechanical properties, etc., could be found in our previously published work (Ref 1).

To evaluate the adhesion strength of the four coatings, scratch tests were undertaken using a Macro-Scratch tester (CSM Revestest, Switzerland) employing a diamond Rockwell C indenter (with a radius of 200 μm). A preload of 1 N was applied, then a progressive load, at a loading rate of 100 N/min, was applied to the indenter. A constant scratch velocity of 3.36 mm/min was used. The load range of 1-100 N was applied for all measurements. For each sample, at least 4 scratch tests were conducted. During the scratch tests both the friction force and acoustic emission were acquired simultaneously.

The tribological properties of the coatings were studied using a reciprocating tribometer (MFT-EC4000) under an ambient atmosphere (65% humidity, room temperature). An alumina ball, 6 mm in diameter, was employed as the counter body. The reciprocating frequency was set at 2 Hz, the applied normal load was 2 N and the stroke length was 5 mm. The total sliding distance was 10 m. At least two tests were conducted for each parameter setting. The wear rate (k) of the coatings was estimated from the expression:

$$k = V/(F \cdot L)$$

where F is the applied normal load, L is the total sliding distance and V is the wear volume.

The scratch and wear tracks for each sample were characterized using an optical microscope (Leica-DMi8C), together with a multi-functional tester for material surface properties operating as surface profilometer (MFT-4000, China) and a scanning electron microscope (SEM) (Phenom XL G2). Chemical analysis of the scratch tracks and wear tracks were undertaken by energy dispersive x-ray spectroscopy (EDS) using a system attached to the SEM.

3. Results

Figure 1 shows the representative friction coefficients (CoF) curves, as a function of distance along the scratch track, for the four coatings under investigation following scratch testing. A general increase in CoF values was noticed with increasing applied normal load for all four coatings. It has been suggested that the increase in friction coefficient at higher loads can be attributed to the increasing contribution of plowing (as well as plasticity) to the overall experimentally determined friction forces as both the applied scratch load and depth of the scratch track increase (Ref 25). However, the inflections of the CoF curves, as marked by arrows in Fig. 1, suggest that the indenter begins at that point to interact with the underlying substrate. According to Fig. 1, the CoF inflection for CoCrNi1 was located at around 2 mm along the scratch track, compared to a location of ~ 1 mm for CoCrNi3. In addition, it can be seen that the turning-point of the CoF for both coatings containing the Ti wetting layer occurred at a much shorter scratch distance $(\sim 0.6 \text{ mm}).$

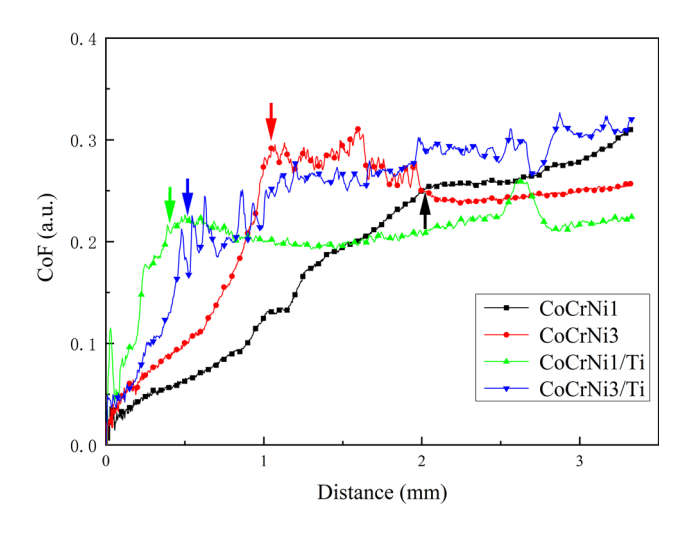


Fig. 1 Representative friction coefficient of the CoCrNi-based coatings during progressive scratching. Arrows indicate the inflection of the CoF curves

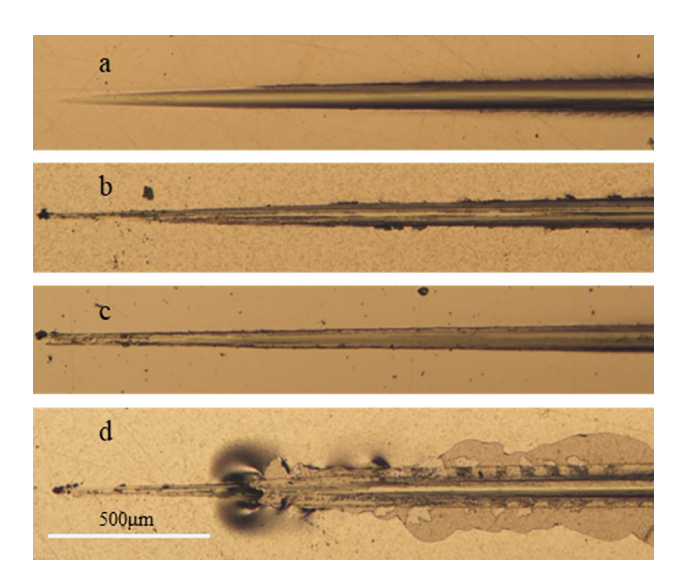


Fig. 2 Optical images of the scratch tracks (loading range 1-65 N) of (a) CoCrNi1, (b) CoCrNi3, (c) CoCrNi1/Ti and (d) CoCrNi3/Ti

Figure 2 shows representative optical images of the scratch track for all four coatings for a region corresponding to the initial application of an applied load to a load of 65 N (i.e the first ~ 2.1 mm of the scratch track). It appears to be that no apparent coating cracking, chipping or spallation can be observed along the scratch track up to an applied load of 65 N for CoCrNi1, CoCrNi3 and CoCrNi1/Ti (as shown in Fig. 2a, b and c, respectively). By contrast, for CoCrNi3/Ti, when the applied load exceeds 16 N (corresponding to a travel distance of ~ 0.6 mm), significant coating delamination along the flanks of the scratch track and cracking of the coating was observed along the scratch track (Fig. 2d).

Figure 3 presents a secondary electron image and EDS elemental maps of a series of scratch tracks for CoCrNi1. According to Fig. 3(b), (c) and (d), the signal intensities for Ni, Cr and Co are gradually weakened along the scratch tracks, and the eventual dark contrast suggesting an absence of these elements becomes readily noticeable at a scratch distance of ~ 1.6 mm (corresponding to a normal applied load of

 \sim 49 N). Correspondingly, the signal for Fe (Fig. 3e), originating from the substrate, gradually intensifies as a result of the gradual thinning of the coating. It is also evident that the intensification in Fe signal mirrors the reduction in signals for Co, Cr and Ni.

By contrast, the CoCrNi layer of the CoCrNi1/Ti coating had been completely removed at a scratch distance of ~ 0.7 mm (Fig. 4), as the signals for Ni, Co and Cr could no longer be detected when the distance along the scratch track exceeded 0.7 mm. Interestingly, the Ti signal is still clearly evident in the scratch track after the removal of the outmost CoCrNi layer. This phenomenon may indicate a stronger adhesion strength at the Ti wetting layer/M2 substrate interface than that at the Ti wetting layer/CoCrNi layer interface.

Figure 5 shows the EDS elemental maps for CoCrNi3/Ti at the location where severe coating spallation began to occur. Again, an intense Ti signal can be detected in the coating failure region, while the signals for Co, Cr and Ni are barely detected. This, in turn, supports the weak adhesion bond strength at the Ti wetting layer/ CoCrNi outmost layer interface, as noted above for CoCrNi1/Ti.

In scratch testing, there are two critical loads, L_{c1} and L_{c2}, which are widely accepted as a measure of a coating's cohesive and interfacial adhesive strength, corresponding, respectively, to the initial onset of coating cracking (L_{c1}) and then substrate exposure (L_{c2}) (Ref 26). Due to the excellent ductility of the CoCrNi coatings, no coating cracking could be readily observed along the scratch tracks for coatings CoCrNi1, CoCrNi3 and CoCrNi1/Ti when examined by SEM. Hence the L_{c1} values were difficult to precisely determine for these coatings and so are not reported here. In contrast, the Lc2 values were determined to be the load where severe coating spallation occurred, or intense signal from substrate could be detected. Table 1 summarizes the location and the critical loads (L_{c2}) for all four coatings. Clearly, coatings CoCrNi1 and CoCrNi3 possess higher L_{c2} values than the coatings containing a Ti wetting layer. This again implies that the wetting layers for these coatings are not effective in promoting coating/substrate adhesion for these MEA CoCrNi coatings. Moreover, it is found that the L_{c2} value for CoCrNi1 is $\sim 51\,$ N, which is much higher than that for CoCrNi3 (\sim 37 N). This indicates that an increase in CoCrNi layer thickness has a negative effect on the scratch properties of these CoCrNi coatings.

Representative friction coefficient curves of the four coatings tested against an alumina ball as a function of sliding time are presented in Fig. 6. Each curve corresponds to one of the tests for each individual coating. The friction coefficient for all coatings instantly reached a considerably high value, due to the mechanical engagement caused by the asperities at the coating/counter-ball interface during the initial running-in stage (Ref 27). Following this, the friction coefficient for coatings CoCrNi1, CoCrNi3 and CoCrNi1/Ti decreased rapidly from ~ 0.3 to ~ 0.2 within half a minute. Then, the friction coefficient saw a gradual increase to ~ 0.3 and remained at this level until the test is concluded. The friction coefficient for CoCrNi3/Ti fluctuated between ~ 0.3 and ~ 0.35 , before gradually increasing to ~ 0.4 and then remained at this level.

Figure 7 presents the representative wear morphology and corresponding profiles for one of the wear tracks from each individual coating tested under identical condition. From Fig. 7(a), there appears to be some wear debris, evident as dark contrast, remaining in the wear track for CoCrNi1. Meanwhile, the brown-colored contrast in the center of the

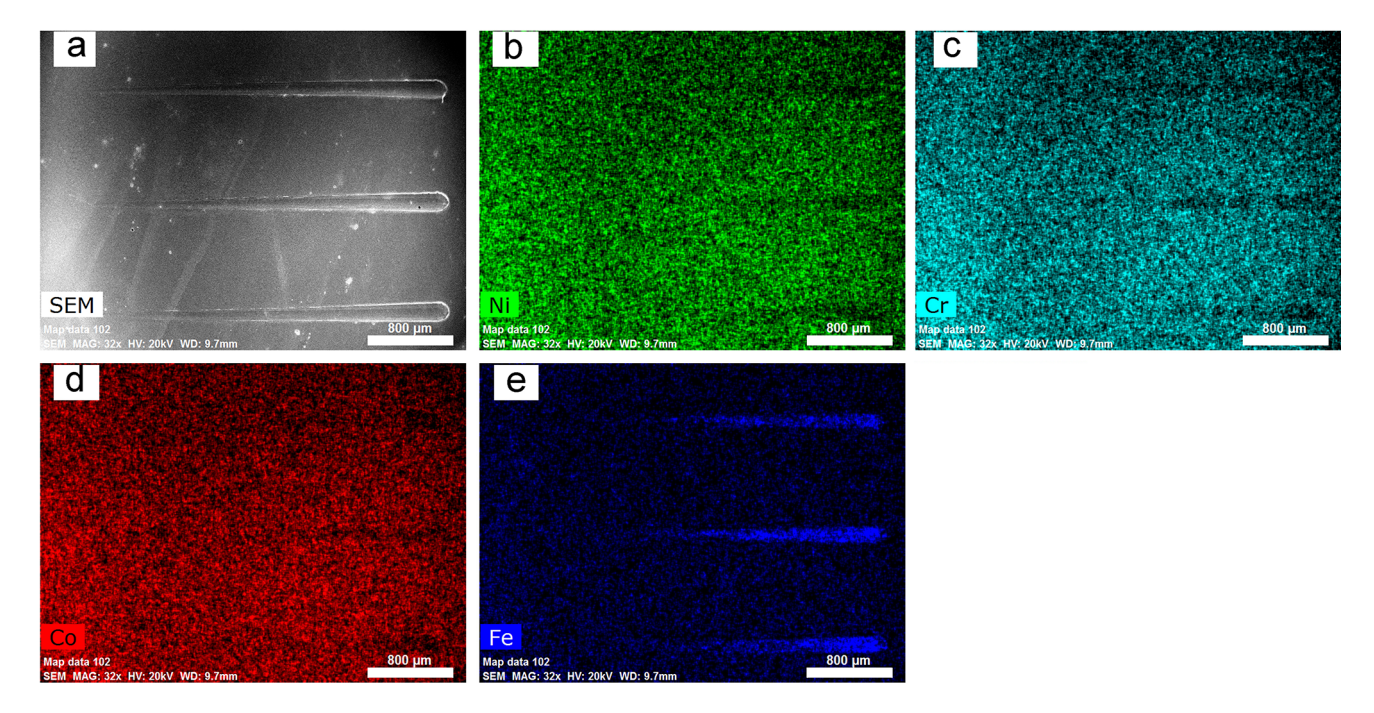


Fig. 3 SEM-EDS analysis of the scratch tracks for coating CoCrNi1: (a) secondary electron image, EDS elemental maps for (b) Ni, (c) Cr, (d) Co and (e) Fe

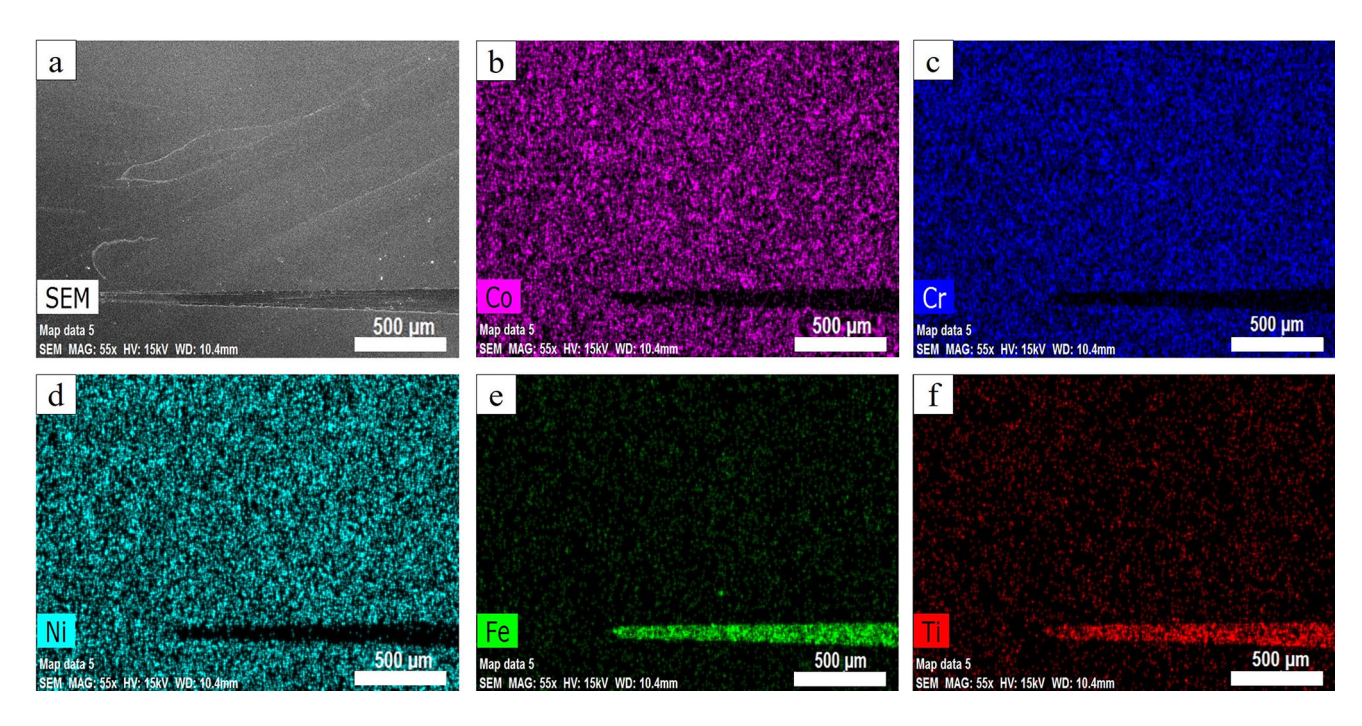


Fig. 4 SEM-EDS analysis of the scratch tracks for coating CoCrNi1/Ti: (a) secondary electron image, EDS elemental maps (b) Co, (c) Cr, (d) Ni, (e) Fe and (f) Ti

wear track may indicate the exposure of substrate, which was later confirmed by SEM-EDS analysis. The wear track is $\sim 338~\mu m$ in width and $\sim 1.4~\mu m$ in depth, indicating the coating was already worn through to the substrate, and the cross-sectional area of the wear track was $\sim 285~\mu m^2$. For CoCrNi1/Ti, compact layers of wear debris could be observed on both sides of the wear track, as shown in the upper image of Fig. 7(b). The wear track is $\sim 336~\mu m$ in width and $\sim 2.0~\mu m$ in depth, with a cross-sectional worn area of $\sim 483~\mu m^2$.

Similarly, the exposure of substrate and accumulation of compact layer of wear debris could also be observed in the wear track for the thick CoCrNi3 coating, as shown in Fig. 7(c). The wear track is $\sim 534~\mu m$ in width and $\sim 2.7~\mu m$ in depth, with a cross-sectional area of $\sim 882~\mu m^2$. For the CoCrNi3/Ti coating (Fig. 7d), however, severe coating spallation had occurred. The afterward wear process was actually done on the substrate, resulting in a very wide profile curve. The cross-sectional worn area and the wear rate for all coatings are given

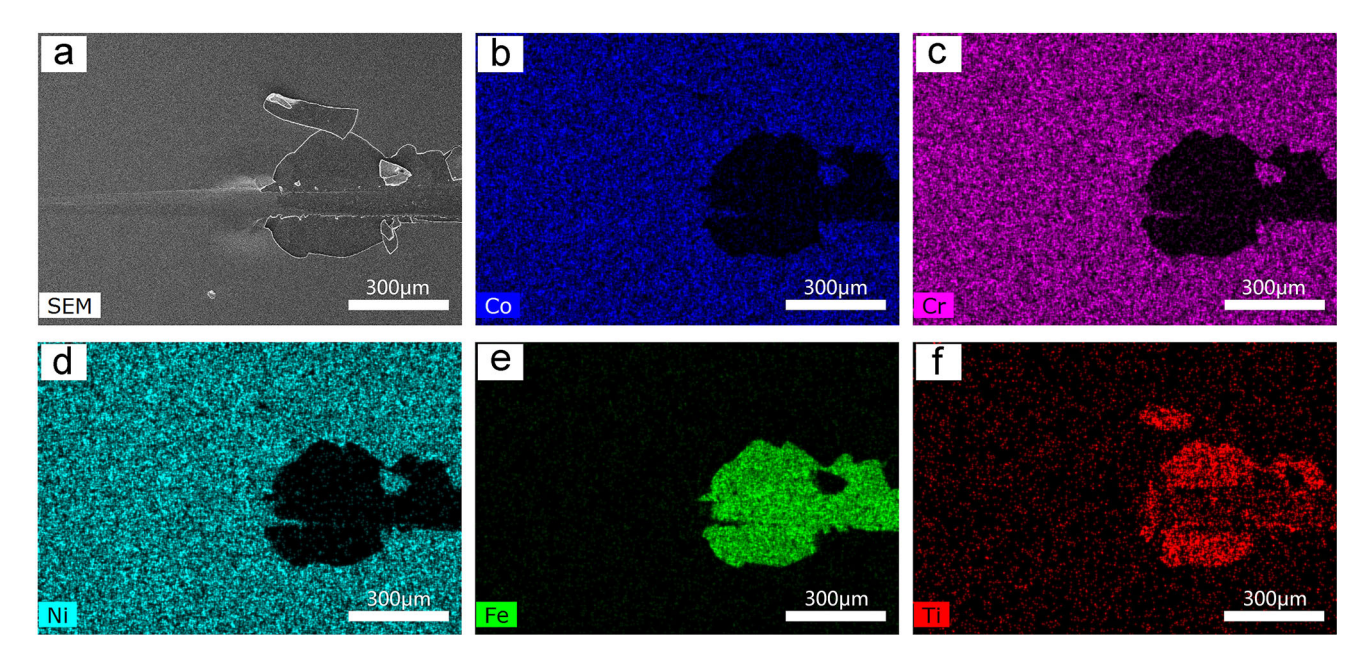


Fig. 5 SEM-EDS analysis of the scratch tracks for coating CoCrNi3/Ti: (a) secondary electron image, EDS elemental maps (b) Co, (c) Cr, (d) Ni, (e) Fe and (f) Ti

Table 1 The critical load, Lc2, and its corresponding location, for all four coatings

Sample	Critical load (Lc2), N	Location, mm	
CoCrNi1	~ 51	1.7	
CoCrNi3	~ 37	1.2	
CoCrNi1/Ti	~ 21	0.7	
CoCrNi3/Ti	~ 16	0.6	

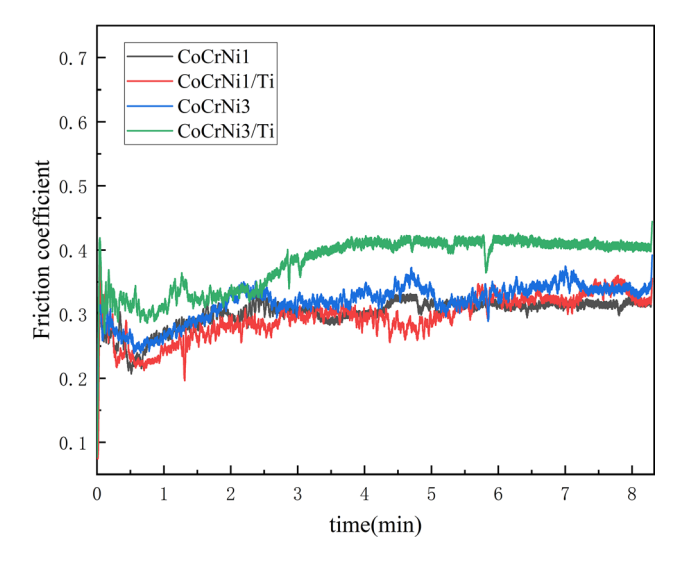


Fig. 6 Friction curves of the four samples as a function of sliding distance against a Al₂O₃ ball under a constant normal load of 5 N

in Table 2. It should be noted that the calculated wear rate for the thinner coatings (CoCrNi1 and CoCrNi1/Ti), given in Table 2, might underestimate the true wear rate of both coatings since wear progressed into the steel substrate. Conversely, the

wear rate of the CoCrNi3/Ti coating might be overestimated because of the large exposed area resulting from coating spallation.

Figure 8 shows the EDS elemental maps of the wear track for CoCrNi1. It is clear that the outmost CoCrNi layer was removed in the wear track since the signals of Cr, Co and Ni can barely be detected in this area, while there are a few islands of compact wear debris observed on both sides of the wear track. From the observed distribution of Cr, Co, Ni and O, it is believed that these compact layers are composed of mixtures of oxides such as CrOx, CoOx and NiOx, due to tribo-chemical reactions during wear testing. Similar observations have been recorded elsewhere (Ref 24, 28). Additionally, the detection of O in the central area of the wear track might suggest that oxidation of the substrate had taken place after removal of the CoCrNi layer through the wear test. The SEM-EDS analysis of the wear tracks for CoCNi3 and CoCrNi1/Ti showed similar characteristics as that observed for CoCrNi1 (as shown in Fig. 8). Therefore, for brevity, the corresponding SEM images and elemental maps are not shown here.

Figure 9 shows the SEM image and EDS elemental maps for the CoCrNi3/Ti wear track. The compact layer, appearing with dark contrast, in the wear track is mainly comprised of oxides including CrO_x, CoO_x and NiO_x. Since severe coating failure had occurred during wear testing, oxidation of the substrate following removal of the CoCrNi and Ti layers was also evident. According to the elemental maps, the surface area surrounding the wear track can be split into three distinct regions. In region I, the substrate is completely exposed, while in region II the Ti wetting layer remains and in region III the coating is intact.

4. Discussion

As shown in Table 1, the CoCrNi coatings without a 100 nm Ti interlayer showed much better adhesion strength than those containing a Ti interlayer. A comparison between Fig. 3 and 5

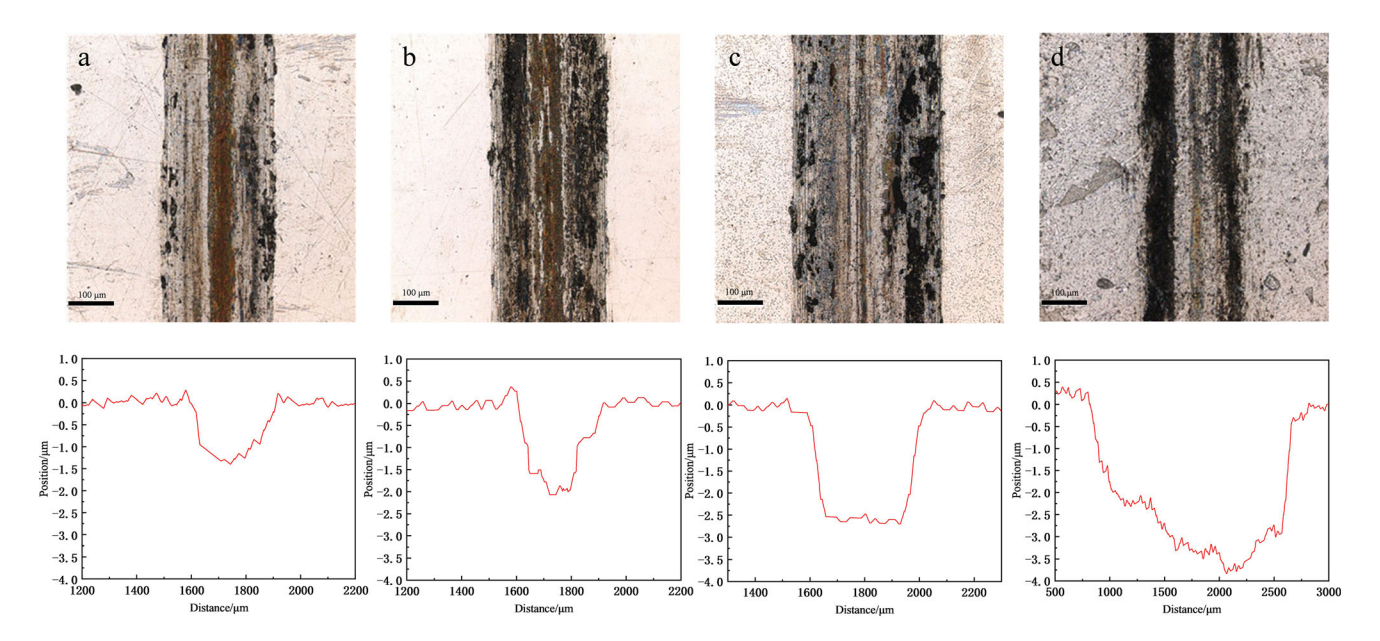


Fig. 7 3D laser confocal image and corresponding profile of the wear track for different coatings under identical test conditions: (a) CoCrNi1, (b) CoCrNi1/Ti, (c) CoCrNi3, (d) CoCrNi3/Ti

Table 2 Wear rates for the coatings CoCrNi1, CoCrNi1/Ti and CoCrNi3

Coatings	CoCrNi1	CoCrNi1/Ti	CoCrNi3	CoCrNi3/Ti
Cross-sectional worn area, μ m ²	285	483	882	5030
Wear rate (× 10 ⁻⁵ mm ³ /N m)	7.125	12.075	22.05	125.75

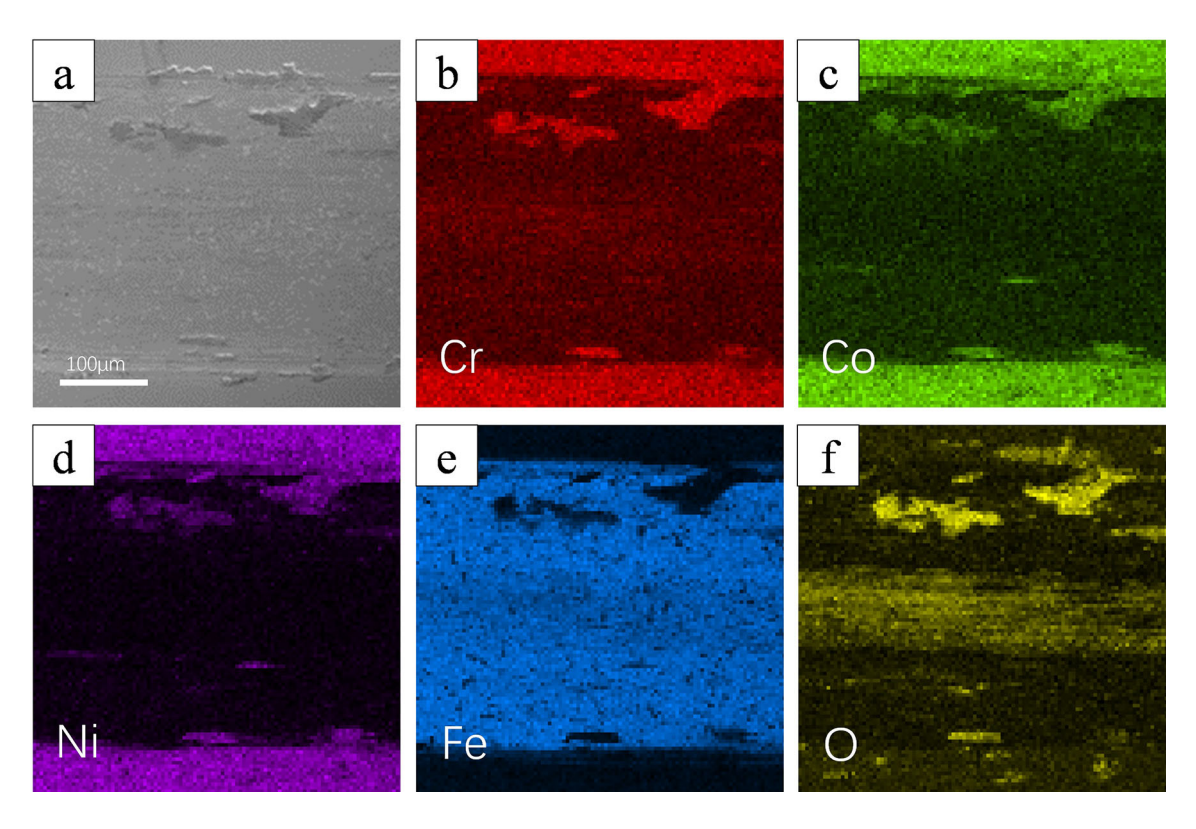


Fig. 8 SEM-EDS analysis of the wear track for CoCrNi1: (a) back scattered electron image, elemental maps for (b) Cr, (c) Co, (d) Ni, (e) Fe and (f) O

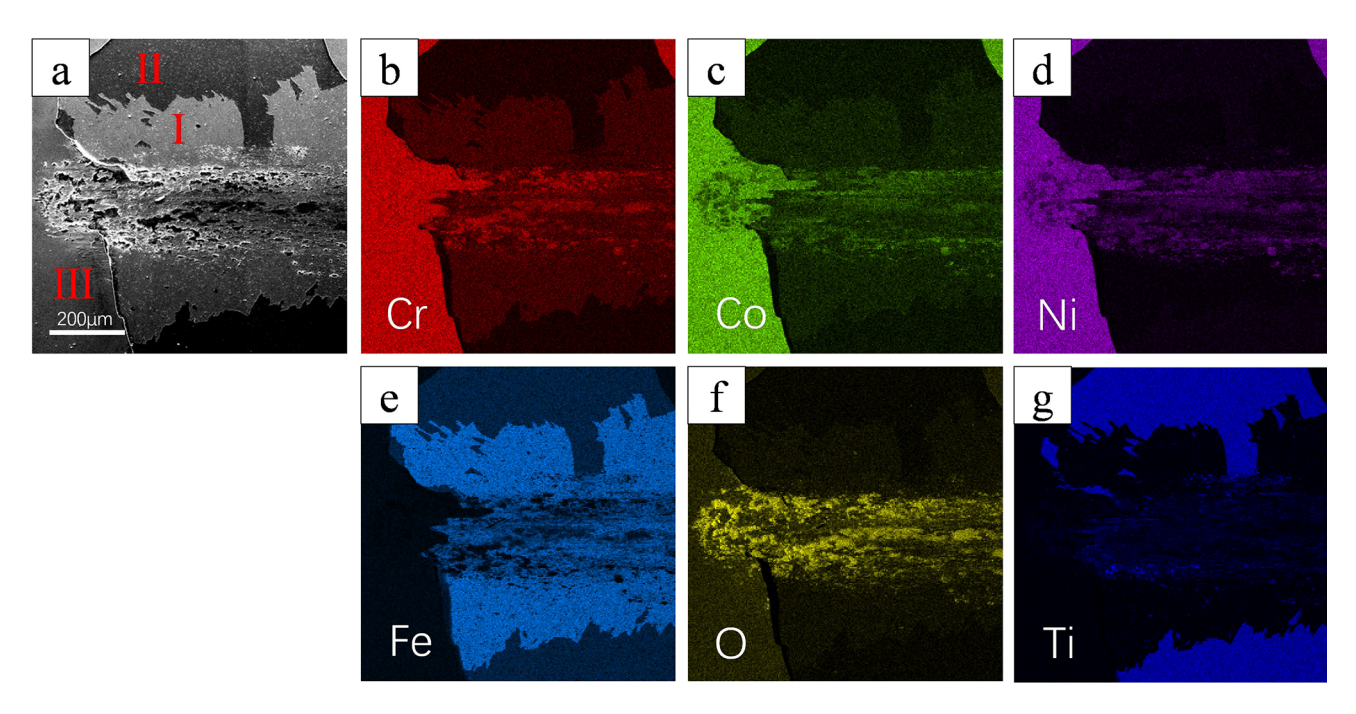


Fig. 9 SEM-EDS analysis of the wear track for CoCrNi3/Ti: (a) secondary electron image, elemental maps for (b) Cr, (c) Co, (d) Ni, (e) Fe, (f) O and (g) Ti

indicates the adhesive strength at the CoCrNi/steel substrate interface is much stronger than the adhesive strength at the CoCrNi/Ti interlayer interface. Therefore, it seems the inclusion of the Ti interlayer negatively influences the adhesive strength. It is assumed that there are two reasons for this degradation in adhesive strength. Firstly, the elements Fe, Co and Ni are close in atomic number, which might facilitate the interdiffusion at the CoCrNi/steel substrate interface during the non-equilibrium film growth process (Ref 29, 30). Consequently, the CoCrNi coatings without Ti interlayer showed better adhesive strength. Secondly, it has been suggested that differences in hardness may greatly influence adhesive strength (Ref 21). To optimize the adhesion response of a coating, the hardness of the interlayer, if introduced, should be similar in value to the substrate hardness. It has been reported the hardness values for the CoCrNi coating, M2 steel and magnetron sputtered Ti layer are, respectively, 10.0 GPa (Ref 1), 8.8 GPa (Ref 31) and 7.9 GPa (Ref 32). Clearly, the hardness mismatch between CoCrNi and M2 is much smaller than the difference in hardness values between the CoCrNi coating and the sputtered Ti interlayer. This also implies stronger adhesion at the CoCrNi/M2 interface than the CoCrNi/ Ti interface. In addition, the strong adhesion between the sputtered Ti layer and M2 substrate, which can be supported by the evidence in Fig. 4 and 5, may arise from the close match in their hardness values.

In addition to the effects arising from the presence of the interlayer, the coating thickness also influences the scratch behavior of the coatings. According to Table 1, for the CoCrNi coatings directly deposited on the M2 substrate, the critical load $L_{\rm c2}$ for the thinner CoCrNi1 coating (~ 51 N) is much higher than that for the thicker CoCrNi3 coating (~ 37 N). Similarly, for the CoCrNi coatings containing a Ti interlayer, the critical load $L_{\rm c2}$ for CoCrNi1/Ti (~ 21 N) is also slightly higher than that for CoCrNi3/Ti (~ 16 N). Therefore, the critical load $L_{\rm c2}$ appears to decrease with increasing coating thickness. It has

been proposed that the coating thickness determines the stress field distribution under contact loading (Ref 33). Indeed, in our previous studies, these coatings were subjected to nanoindentation testing under a maximum applied load of 500 mN using a spherical indenter (radius: 5 μ m) (Ref 1). The cross-sectional secondary electron images showed that for CoCrNi1 and CoCrNi1/Ti the applied load was distributed across both the coating and substrate, since severe plastic deformation in both the coating and the substrate was observed without any delamination or cracks. Conversely, for the thicker CoCrNi3 and CoCrNi3/Ti coatings, the applied load was mainly absorbed by the coating and only a limited amount of the applied plastic deformation appeared to be transmitted into the substrate. Accordingly, for the present scratch tests, the load imposed by the moving probe can be shared by plastic deformation occurring in both coating and substrate for the thin CoCrNi1 coating. While for the thicker CoCrNi3 coating, the damage is mostly accumulated within the coating, rather than the substrate, leading to earlier exposure of the substrate. By contrast, the inferior performance of CoCrNi1/Ti and CoCrNi3/ Ti can be associated with the introduction of Ti interlayer, as discussed above.

As shown in Fig. 6, the average friction coefficients for CoCrNi1, CoCrNi1/Ti and CoCrNi3 coatings was around 0.3, which was comparable to the friction coefficients determined for laser cladded CoCrNi-based composite coatings (ranging from 0.3 to 0.4) (Ref 34). On the other hand, the friction coefficient was just above 0.3 for the CoCrNi3/Ti coating during the early stages of testing, which then readily increased to 0.4. This rapid transition in friction coefficient might suggest a variation in sliding contact conditions. Post optical and SEM analysis, as shown in Fig. 7(d) and 9, confirmed the premature coating failure during reciprocating wear testing.

From analysis of the friction coefficients (Fig. 6) and the wear track features (Fig. 7, 8 and 9) of all the coatings might suggest that the principal wear mechanism for CoCrNi1,

CoCrNi1/Ti and CoCrNi3 coatings was abrasive wear for the presence of long wear grooves in the wear tracks for these coatings, while fracture wear played a more dominant role for CoCrNi3/Ti. In fact, tribo-oxidation can take place during wear testing since oxygen arising from ambient air was associated with the reaction, resulting in the formation of oxide wear debris and an oxidized surface (Ref 35). In addition, repeated sliding will lead to the accumulation and compaction of some of the oxide wear debris into thick compact oxide transfer layers attached on the wear tracks for all coatings, as shown in Fig. 7, 8 and 9, which means that minor adhesive wear occurs for all these coatings. The presence of compact oxide layers will lead to fluctuations in friction coefficient during wear rest. Moreover, it has been suggested that the fractured oxides can serve as a third body in the tribological system and may result in an increase in wear volume (Ref 6).

By comparing the wear rates of the CoCrNi1, CoCrNi1/Ti and CoCrNi3 coatings (as presented in Table 2), the thinner coatings, CoCrNi1 and CoCrNi1/Ti, demonstrated qualitatively better wear resistance than the thicker CoCrNi3 coating. The average wear rate of the thinner coatings (CoCrNi1 and CoCrNi1/Ti) was around 9.6×10^{-5} mm³/Nm, which is only 38% of the wear rate of a resistance seam processed MEA CoCrNi coating $(2.47 \times 10^{-4} \text{ mm}^3/\text{Nm})$ reported by Zhao et al. (Ref 24). Further, the introduction of a 100 nm Ti interlayer into the CoCrNi1 resulted in a reduction in wear resistance. The wear rate of coatings may be influenced by both external and internal causes (Ref 36, 37). As the wear test experimental conditions were identical, the influence of any external factors on the wear response of the CoCrNi and/or CoCrNi/Ti coatings may be ignored. The influence of internal factors, such as hardness, coating thickness and residual stress of the CoCrNi coatings on the wear response therefore need to be considered.

The mechanical properties and residual stresses of these coatings are summarized in Table 3 based on our previous study (Ref 1), where the residual stress was analyzed using an X'pert MRD-Philips diffractometer with psi-goniometer geometry and calculated by employing the conventional $\sin^2 \psi$ method. H/E and H³/E² are two important parameters, which are often used, respectively, to represent a material's elastic strain to failure and resistance to plastic deformation. The ratios H/E and H³/E² have been regarded as the indicators of the wear resistance for thin films (Ref 38). In this current investigation, hardness, the H/E and H³/E² ratios are similar for all coatings, and as a consequence, the hardness and H/E ratio should not be key factors in determination of the relative wear rate of these coatings. Our statement is in great agreement with the literature reported by Lin et al. (Ref 20). They investigated the wear resistance of TiZrN/Ti coatings with comparable hardness and H/E ratios, and argued both were not the significant factors contributing to the wear rate of these TiZrN-based coatings.

According to Table 2 and 3, the thinner CoCrNi1 coating, which also possesses the highest level of compressive residual stress, demonstrates the best wear resistance. While, the thicker CoCrNi3 coating and CoCrNi1/Ti show inferior wear resistance. Thus, factors such as the residual stress and coating thickness might both play a role on the wear rate of these coatings. Clearly, by comparison with CoCrNi1, the introduction of a 100 nm Ti interlayer into the 1 μm CoCrNi coating decreases the residual compressive stress in the CoCrNi1/Ti coating. Moreover, the residual stress also decreases with an increase in the coating thickness. Similar observation has been reported in sputtered TiN coatings, where the thinnest coating has the highest compressive stress and the compressive residual stresses in the TiN coatings decrease with coating thickness (Ref 39). It is believed that a higher level of compressive residual stress in the coating can offset, to a certain extent, the tensile stress generated during the wear test, and thus, inhibit initiation and propagation of the cracks on the coating surface (Ref 40). Therefore, the wear resistance increases with increasing compressive residual stress demonstrating that the coating is well bonded with its underlying substrate. Similar results can also be found elsewhere. For instance, Luo et al. found that the wear loss decreased with an enhancing value of the compressive stress in HVOF-sprayed WC-12Co coatings (Ref 41). Moreover, Alanzazi et al. observed that the wear resistance of the electrodeposited cobalt-phosphorus-based coatings improved with increasing compressive residual stress (Ref 42).

As for the CoCrNi3/Ti coating, it is suggested that the introduction of the Ti interlayer reduces the adhesion strength and contributes to the fracture-dominated wear of this coating. Indeed, CoCrNi3/Ti possessed the lowest adhesion strength as noted above. The accumulated strains during continuous sliding could readily induce spallation of the CoCrNi3/Ti coating, even though the CoCrNi layer itself demonstrates superior fracture toughness. The result is in good agreement with observations in the literature, where wear resistance can be closely related with adhesion strength (Ref 43, 44).

5. Conclusions

In this study, scratch and wear tests were performed on 1 and 3 μ m thick MEA CoCrNi coatings with and without a 100 nm Ti interlayer. It was found that the critical load L_{c2} decreased with an increase in CoCrNi coating thickness, and an introduction of Ti interlayer was detrimental for the scratch adhesion strength compared with the samples without interlayer. In terms of the wear mode, the abrasive wear was found to be the major wear mechanism for the CoCrNi1, CoCrNi1/Ti and CoCrNi3 coatings, while fracture wear was dominant for

Table 3 Mechanical properties and the calculated residual stresses of the coatings (Ref 1)

Sample	Hardness (H), GPa	Elastic modulus (E), GPa	H/E	H ³ /E ² , GPa	Calculated residual stress, MPa
CoCrNi1	10.0 ± 0.83	248.8 ± 14.1	0.0401	0.0162	-1101.4 ± 166
CoCrNi3	9.6 ± 0.66	250.0 ± 12.4	0.0384	0.0142	-335.2 ± 84
CoCrNi1/Ti	9.0 ± 0.36	231.2 ± 8.9	0.0389	0.0136	-571.4 ± 113
CoCrNi3/Ti	9.4 ± 0.43	236 ± 10.5	0.0398	0.0149	-497.2 ± 66

the CoCrNi3/Ti coating. Nonetheless, minor adhesive wear was observed to occur for all four coatings. In general, the thinner CoCrNi coatings demonstrated better wear resistance than their thicker counterparts. The mechanical properties of these coatings, such as hardness, H/E and H³/E², were not the key factors in determination of the relative wear resistance for these coatings. Rather it is suggested that residual compressive stress and coating thickness may have played a more important role in determining the wear resistance of these MEA coatings. It was found that increasing residual compressive stress was beneficial to the wear resistance of these coating. An increase in MEA CoCrNi coating thickness and/or an introduction of Ti interlayer decreased the residual compressive stress, and consequently had a negative impact on the wear resistance of the MEA CoCrNi coatings.

Acknowledgment

This study is supported by the Australian Research Council Discovery Project (DP200103152), the Open Fund of the Hubei Longzhong Laboratory (Project No. 2022KF-11), Innovation and Entrepreneurship Plan of Jiangsu Province and the startup fund for advanced talents of Jiangsu University. F. Cao appreciates the support by UNSW Science PhD writing scholarship.

Conflict of interest

The authors have no conflict to disclose.

References

- F. Cao, P. Munroe, Z. Zhou and Z. Xie, Medium Entropy Alloy CoCrNi Coatings: Enhancing Hardness and Damage-Tolerance Through a Nanotwinned Structuring, Surf. Coat. Technol., 2018, 335, p 257–264.
- F. Cao, P. Munroe, Z. Zhou and Z. Xie, Microstructure and Mechanical Properties of a Multilayered CoCrNi/Ti Coating with Varying Crystal Structure, Surf. Coat. Technol., 2018, 350, p 596–602.
- C. Yin, H. Huang, J. Qin, B. Zheng, X. An and Y. Yi, Microstructure, Mechanical and Tribological Properties of Thermomechanical Processed (CoNiCr_{0.5})₉₅Al_xTiy High-Entropy Alloys, *J. Mater. Res. Technol.*, 2023, 25, p 1761–1773.
- X. Sun, H. Zhang, S. Lu, X. Ding, Y. Wang and L. Vitos, Phase Selection Rule for Al-Doped CrMnFeCoNi High-Entropy Alloys from First-Principles, *Acta Mater.*, 2017, 140, p 366–374.
- J. Yang, K. Zhao, G. Wang, C. Deng, N. Liu, W. Zhang and J. Yang, Influence of Coating Thickness on Microstructure, Mechanical and LBE Corrosion Performance of Amorphous AlCrFeTiNb High-Entropy Alloy Coatings, Surf. Coat. Technol., 2022, 441, p 128502.
- T.-C. Huang, S.-Y. Hsu, Y.-T. Lai, S.-Y. Tsai and J.-G. Duh, Effect of NiTi Metallic Layer Thickness on Scratch Resistance and Wear Behavior of High Entropy Alloy (CrAlNbSiV) Nitride Coating, Surf. Coat. Technol., 2021, 425, p 127713.
- J. Yi, L. Yang, S. Tang, F. Cao, M. Xu and L. Wang, Overcoming the Strength-Plasticity Trade-off in a Multi-phase Equiatomic CrCuNiTiV 3D Transition Metal High-Entropy Alloy, *Metall Mater Trans A*, 2021, 52, p 3600–3608.
- P. S. Deshmukh, G. D. Sathiaraj, Microstructure, Mechanical Properties, and Strain Rate Sensitivity of Vacuum Arc Melted CoCrNi Medium Entropy Alloy, *Mater. Today: Proc.*, 2023
- J. Duan, L. Li, Y. Tong, Z. Chen, D. Deng, J. Liu, Z. Cai and H. Wang, Core-Shell Structured h-BN@Ni Reinforced CoCrNi-Based Self-Lubricating Composites, Surf. Coat. Technol., 2022, 448, p 128939.
- Y.-S. Lin, Y.-C. Lu and C.-H. Hsueh, Strengthening of CoCrNi Medium Entropy Alloy with Gadolinium Additions, *Vacuum*, 2023, 211, p 111969.

- S. Pan, C. Zhao, P. Wei and F. Ren, Sliding Wear of CoCrNi Medium-Entropy Alloy at Elevated Temperatures: Wear Mechanism Transition and Subsurface Microstructure Evolution, Wear, 2019, 440–441, p 203108
- B. Song, Y. Hua, C. Zhou, Y. Li, L. Yang and Z. Song, Fabrication and Anticorrosion Behavior of a Bi-Phase TaNbHfZr/CoCrNi Multilayer Coating through Magnetron Sputtering, *Corros. Sci.*, 2022, 196, p 110020
- Y. Feng, K. Feng, Y. Feng and Z. Li, Influence of Residual Stress on the Cracking of the Laser-Cladded High-Hardness Coating, *Mater. Lett.*, 2023, 349, p 134715.
- C. Liu, X. Qiu, J. Peng and Z. Wang, Structure and Properties of Laser Cladding CoCrNi Multicomponent Alloy Coating Used in Rain Gauge, Opt. Lasers Eng., 2023, 163, p 107458.
- X. Shang, Z. Wang, X. Wu, Q. Liu, Y. Guo, K. Ding and T. Liao, Laser Cladding [Cr–Fe₄Co₄Ni₄]Cr_{2.6-x}Al_xMo_{0.4} High-Entropy Alloy Coating to Strong-Acid Erosion, *Intermetallics*, 2023, 156, p 107847.
- D. Wang, Q. Hu and X. Zeng, Residual Stress and Cracking Behaviors of Cr₁₃Ni₅Si₂ Based Composite Coatings Prepared by Laser-Induction Hybrid Cladding, Surf. Coat. Technol., 2015, 274, p 51–59.
- Q. Zhu, X. Zhou, F. Yang, Y. Ji, Y. Kong, A. Bi, Z. Zhou, X. Wang, R. Wang, Z. Zhang and X. Jiang, Microstructure Formation, Corrosion Properties, and Tribological Properties of Laser-Cladded CrCoNi Medium-Entropy Alloy Coatings, *Mater. Lett.*, 2023, 347, p 134649.
- S.J. Tsianikas, Y. Chen and Z. Xie, Deciphering Deformation Mechanisms of Hierarchical Dual-Phase CrCoNi Coatings, *J. Mater. Sci. Technol.*, 2020, 39, p 7–13.
- J. Musil and J. Vlček, A Perspective of Magnetron Sputtering in Surface Engineering, Surf. Coat. Technol., 1999, 112, p 162–169.
- Y.-W. Lin, P.-C. Chih and J.-H. Huang, Effect of Ti Interlayer Thickness on Mechanical Properties and Wear Resistance of TiZrN Coatings on AISI D2 Steel, Surf. Coat. Technol., 2020, 394, p 125690.
- P. Lu, H. Gomez, X. Xiao, M. Lukitsch, D. Durham, A. Sachdeve, A. Kumar and K. Chou, Coating Thickness and Interlayer Effects on CVD-Diamond Film Adhesion to Cobalt-Cemented Tungsten Carbides, Surf. Coat. Technol., 2013, 215, p 272–279.
- S.J. Bull, P.R. Chalker, C.F. Ayres and D.S. Rickerby, The Influence of Titanium Interlayers on the Adhesion of Titanium Nitride Coatings Obtained by Plasma-Assisted Chemical Vapour Deposition, *Mater. Sci. Eng. A*, 1991, 139, p 71–78.
- M. Abdoos, K. Yamamoto, B. Bose, G. Fox-Rabinovich and S. Veldhuis, Effect of Coating Thickness on the Tool Wear Performance of Low Stress TiAlN PVD Coating during Turning of Compacted Graphite Iron (CGI), Wear, 2019, 422–423, p 128–136.
- D. Zhao, D. Kong, J. Huang, M. Wang and T. Yamaguchi, Characterization and Wear Behavior of CoCrNi Medium Entropy Alloy Coating on Al Alloy by Resistance Seam Processing, *Mater. Trans.*, 2022, 63, p 649–654.
- B. Beake, V. Vishnyakov and A. Harris, Relationship Between Mechanical Properties of Thin Nitride-Based Films and Their Behaviour in Nano-Scratch Tests, *Tribol. Int.*, 2011, 44, p 468–475.
- S. Sveen, J.M. Andersson, R. M'Saoubi and M. Olsson, Scratch Adhesion Characteristics of PVD TiAlN Deposited on High Speed Steel, Cemented Carbide and PCBN Substrates, Wear, 2013, 308, p 133–141.
- M. Federici, C. Menapace, A. Moscatelli, S. Gialanella and G. Straffelini, Effect of Roughness on the Wear Behavior of HVOF Coatings Dry Sliding Against a Friction Material, *Wear*, 2016, 368–369, p 326–334.
- Y. Liu, F. Zhang, Z. Huang, Q. Zhou, Y. Ren, Y. Du and H. Wang, Mechanical and Dry Sliding Tribological Properties of CoCrNiNbx Medium-Entropy Alloys at Room Temperature, *Tribol. Int.*, 2021, 163, p 107160.
- I. Ohnuma, H. Enoki, O. Ikeda, R. Kainuma, H. Ohtani, B. Sundman and K. Ishida, Phase Equilibria in the Fe–Co Binary System, *Acta Mater.*, 2002, 50, p 379–393.
- C.-H. Xia, Y. Wang, J.-J. Wang, X.-G. Lu and L. Zhang, Thermodynamic Assessment of the Co–Fe–Ni System and Diffusion Study of Its FCC Phase, J. Alloys Compd., 2021, 853, p 157165.
- J. Nunes and A.P. Piedade, Nanoindentation of Functionally Graded Hybrid Polymer/Metal Thin Films, Appl. Surf. Sci., 2013, 284, p 792– 797
- 32. N. Arshi, J. Lu, C.G. Lee, J.H. Yoon, B.H. Koo and F. Ahmed, Thickness Effect on Properties of Titanium Film Deposited by D.C.

- Magnetron Sputtering and Electron Beam Evaporation Techniques, *Bull. Mater. Sci.*, 2013, **36**, p 807–812.
- C. Lorenzo-Martin, O. Ajayi, A. Erdemir, G.R. Fenske and R. Wei, Effect of Microstructure and Thickness on the Friction and Wear Behavior of CrN Coatings, *Wear*, 2013, 302, p 963–971.
- D. Jiang, H.-Z. Cui, X.-J. Song, X.-J. Lian, X.-F. Zhao, H. Chen and G.-L. Ma, Wear and Corrosion Resistance of CoCrNi Composite Coatings by Laser Cladding, *China Foundry*, 2022, 19, p 535–543.
- P.W. Shum, W.C. Tam, K.Y. Li, Z.F. Zhou and Y.G. Shen, Mechanical and Tribological Properties of Titanium–Aluminium–Nitride Films Deposited by Reactive Close-Field Unbalanced Magnetron Sputtering, Wear, 2004, 257, p 1030–1040.
- M. Moreno, J.M. Andersson, R. Boyd, M.P. Johansson-Jöesaar, L.J.S. Johnson, M. Odén and L. Rogström, Crater Wear Mechanism of TiAlN Coatings during High-Speed Metal Turning, Wear, 2021, 484

 –485, p 204016.
- A. Mussa, P. Krakhmalev and J. Bergström, Wear Mechanisms and Wear Resistance of Austempered Ductile Iron in Reciprocal Sliding Contact, Wear, 2022, 498–499, p 204305.
- A. Leyland and A. Matthews, On the Significance of the H/E Ratio in Wear Control: A Nanocomposite Coating Approach to Optimised Tribological Behaviour, Wear, 2000, 246, p 1–11.
- Y. Xi, K. Gao, X. Pang, H. Yang, X. Xiong, H. Li and A.A. Volinsky, Film Thickness Effect on Texture and Residual Stress Sign Transition in Sputtered TiN Thin Films, *Ceram. Int.*, 2017, 43, p 11992–11997.
- J. Gunnars and A. Alahelisten, Thermal Stresses in Diamond Coatings and Their Influence on Coating Wear and Failure, Surf. Coat. Technol., 1996, 80, p 303–312.

- W. Luo, U. Selvadurai and W. Tillmann, Effect of Residual Stress on the Wear Resistance of Thermal Spray Coatings, *J. Therm. Spray Technol.*, 2016, 25, p 321–330.
- N.M. Alanazi, A.M. El-Sherik, S.H. Alamar and S. Shen, Influence of Residual Stresses on Corrosion and Wear Behavior of Electrodeposited Nanocrystalline Cobalt-Phosphorus Coatings, *Int. J. Electrochem. Sci.*, 2013, 8, p 10350–10358.
- W. Chen, J. Zheng, Y. Lin, S. Kwon and S. Zhang, Comparison of AlCrN and AlCrTiSiN Coatings Deposited on the Surface of Plasma Nitrocarburized High Carbon Steels, *Appl. Surf. Sci.*, 2015, 332, p 525–532.
- W. Chen, J. Zheng, X. Meng, S. Kwon and S. Zhang, Investigation on Microstructures and Mechanical Properties of AlCrN Coatings Deposited on the Surface of Plasma Nitrocarburized Cool-Work Tool Steels, *Vacuum*, 2015, 121, p 194–201.

Publisher's Note Springer Nature remains neutral with regard to jurisdictional claims in published maps and institutional affiliations

Springer Nature or its licensor (e.g. a society or other partner) holds exclusive rights to this article under a publishing agreement with the author(s) or other rightsholder(s); author self-archiving of the accepted manuscript version of this article is solely governed by the terms of such publishing agreement and applicable law.